Chapter 5

Active Control of Separated Cascade Flow

In this chapter, the possibility of active control using a synthetic jet applied to an unconventional axial stator-rotor arrangement is investigated. Detailed information about the setup of this arrangement and the computational considerations can be found in Section 5.1. Section 5.2 presents the computational results of the unforced arrangement. A synthetic jet of 120Hz located at the natural separation point of the stator blade is composed to manipulate the massive separation on the blades. The results of excitation are described in section 5.3. Section 5.4 gives a general summary of the excitation with a synthetic jet.

5.1 Numerical Setup

It has been shown in Chapter 4 that the synthetic jet is an effective approach to influence the massive separation on a single airfoil at stall angle of attack. The active control can be most efficient when the frequency of excitation has a value in a certain characteristic range. This result, naturally, leads to the thoughts of extending the effectivity of a synthetic jet to the control of the flow field in fluid machines working at part load operation due to the massive separation on the blades.

In this chapter, the possibility is investigated for an unconventional one-stage axial stator-rotor arrangement. The stator and rotor blades are composed of the same NACA63_3-018 airfoil of 0.305 meter length. The detailed setup information is given in Figure 5.1. The stator and rotor have the same vane spacing of 0.3 meter. The stator blades have stagger angles of 50 degrees. The rotor blades have the same stagger angle but are adjusted in the opposite direction. The axial distance between stator and rotor leading edges is 0.365 meter. The setup of the unconventional arrangement aims at the investigation of the features of massive separation in cascade flow and the behavior of a synthetic jet in controlling the massive separation.

In this work, the fluid medium is air. Its density is 1.2kg/m^3, and its dynamic viscosity 1.8×10^{-5} kg/(m·s). The flow comes in from the left at a uniform horizontal velocity of 15m/s with a turbulence degree of 0.25%. Rotor blades are driven to move downward at the velocity of 18m/s. The average incidence angle for the rotor blade is about 22 degrees.

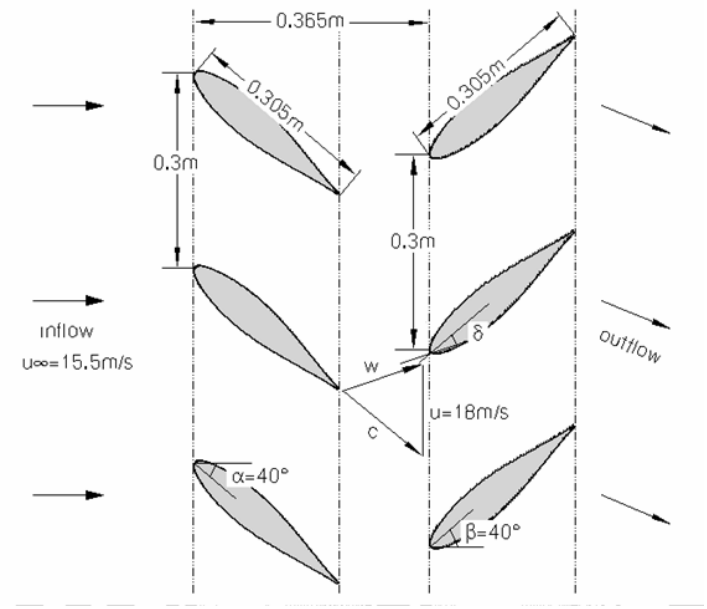

$NACA63_3 - 018$ *blades*

$\rho = 1.2 kg/m^3$

$\mu = 1.8 \times 10^{-5} kg/(m \cdot s)$

$u_\infty = 15.5 m/s$

$Tu = 0.25\%$

Fig. 5.1. Schematic presentation of axial stator-rotor arrangement

The discretization of the computational domain is schematically shown in Figure 5.2. Only one channel of the axial arrangement is simulated as periodic boundary conditions are imposed on the upper and lower boundaries of the computational domain except on the blade surfaces. The grid contains about 152,000 cells. The trailing edges of both blades are locally rounded so that O-grids can be employed. 480 and 440 cells are on the stator and rotor blades, respectively. The first six blocks of the grid are designed for the stator part and do not have relative motion. The other six ones are for the rotor flows and move downward at a velocity of 18m/s.

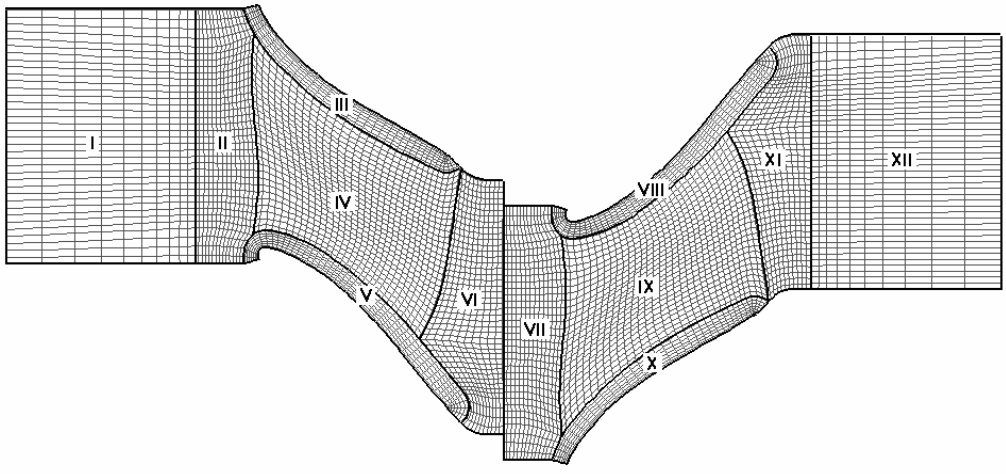

Fig. 5.2. Schematic presentation of grid arrangement

The inlet boundary condition is set at the left side of the computational domain. At the right side of the domain, an outlet boundary condition of zero-gradient is imposed. The upper and lower domain boundaries have the periodic conditions, except on the blade surfaces where the non-slip and impermeable conditions are prescribed.

In the simulation, the flow is treated incompressible. The modified turbulence model described and validated in Chapter 3 is adopted. The near wall region is resolved by Launder-Sharma low-Reynolds-number modification. The grid near the blade surfaces is refined so that y^+ values of the first points away from the airfoil surface are close to unity. The convective fluxes are approximated by the SMART method. The time step is advanced by implicit Euler method. For the sake of convergence, there are hundreds discrete time steps when the moving grid performs one period. Computational accuracy of both velocity components and the pressure is 5×10^{-5}.

5.2 Results without Synthetic Jet

The stator flow is comparable to that of a single airfoil at stall angle of attack. The flow separates directly from the leading edge of the stator blade and cannot reattach onto the blade surface any more. The numerically predicted separation is located very near to the leading edge at 0.1% chord. A large separation region is formed upon the suction side of the stator blades. Inside the region, the fluid recirculates and a large “dead-air” area is formed. The recirculating area induces high level of pressure drag loss and makes the fluid machinery working at extreme part load operation.

The flow has a frequency of 60Hz, as the rotor motion constrains the vortex shedding procedure of the stator flow. Figure 5.3 depicts the flow patterns at four instants in one flow period T_w. These pictures are very similar to the ones of single stalled airfoil. But the height of the separation region is smaller.

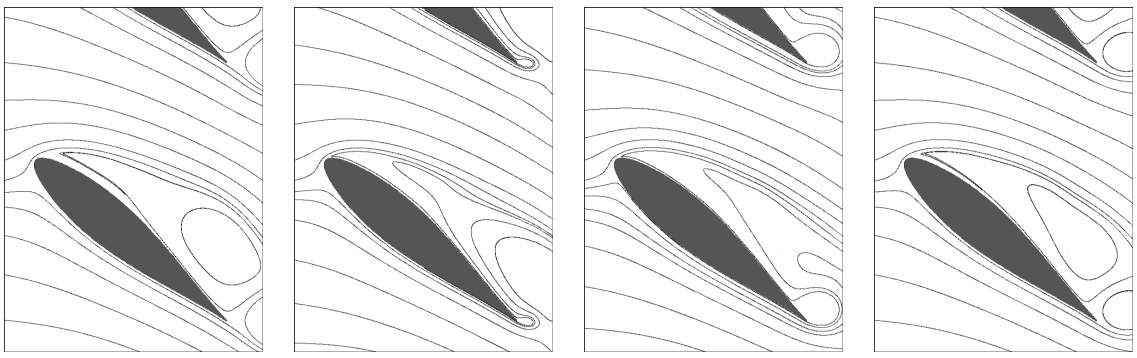

(a) t=0.25T_w (b) t=0.5T_w (c) t=0.75T_w (d) t=1T_w

Fig. 5.3. Stator flow pattern at four instants in one flow period, without control

The rotor blade is located in the stator wake about 0.4 chords downstream of the stator trailing edge. The rotor performance depends strongly on the quality of the stator wake. As a large separation region is formed upon the stator blade and the vortex sheds up periodically, the incident flow for the rotor blade changes its direction in a wide range. It is unsteady and full of turbulent energy. Flow patterns at four instants for the rotor blades are shown in Figure 5.4 where the streamlines are obtained from the relative velocity field. It can be observed that no large separation exists. Instead, recirculating regions are generated periodically at the leading edge. They move downwards along the blade surface. On the other side of the rotor blade, the flow does not separate.

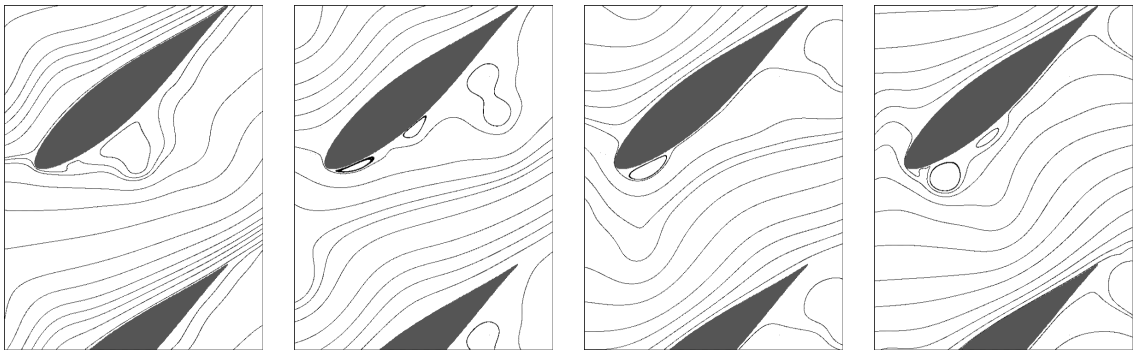

(a) t=0.25T_w (b) t=0.5T_w (c) t=0.75T_w (d) t=1T_w

Fig. 5.4. Rotor flow pattern at four instants in one flow period, without control

As in the case of a single airfoil, the massive separation induces a high level of turbulent energy in the flow field. The distribution of turbulent kinetic energy at eight instants of one flow period is shown in Figure 5.5. Figure 5.6 gives the corresponding pressure coefficient distributions on stator and rotor blades. The turbulent kinetic energy is non-dimensionalized by u_∞^2. The turbulence is of lower level upstream of the stator blade. On the front half of the stator blade, the turbulent kinetic energy is of high level only in the shear layer. The turbulence begins to be amplified from the mid portion of the blade. At the rear part of the large separation region, a high level of turbulent kinetic energy is gathered and shed up periodically in the wake. Another region of high turbulence is induced by the trailing edge and goes into the wake alternatively. The stator wake is dominated by the large scale vortex motions and therefore, the incident flow for the rotor blade is fully turbulent. On the rotor blade, the turbulence structure is developed further in space and tends to be well distributed near the outlet.

In such an arrangement, flow losses are very high because the dominating pressure drag from the massive separation on the stator blade is enormous and the intensive mixing procedure induces also flow losses.

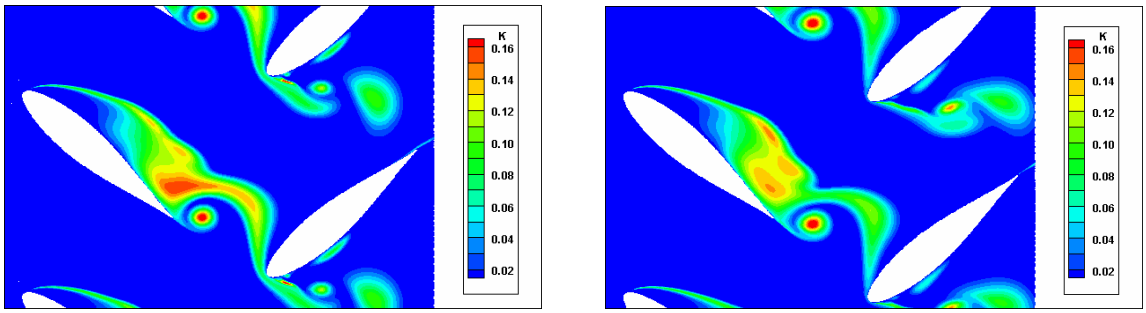

(a) t=0.125T_w (b) t=0.25T_w

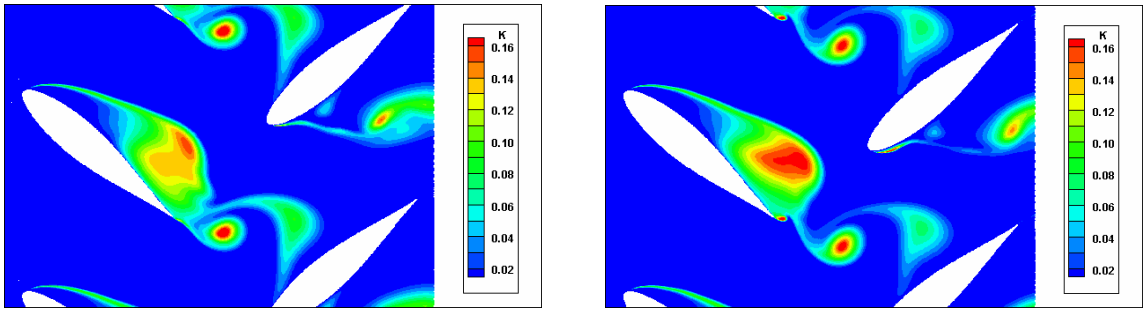

(c) t=0.375T_w (d) t=0.5T_w

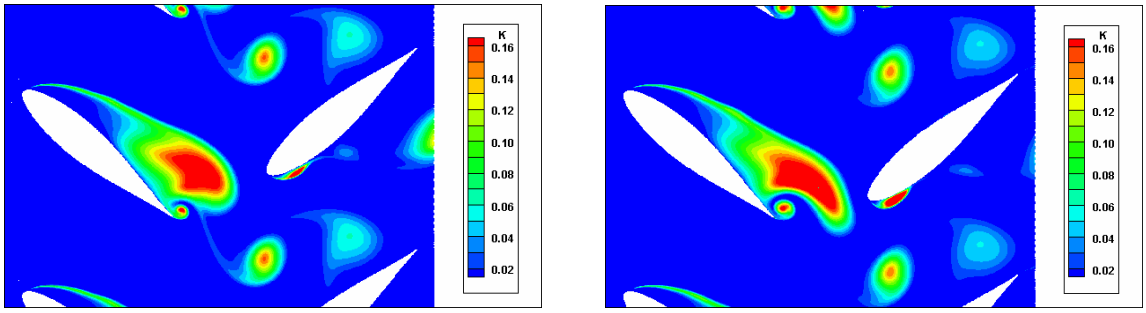

(e) t=0.625T_w (f) t=0.75T_w

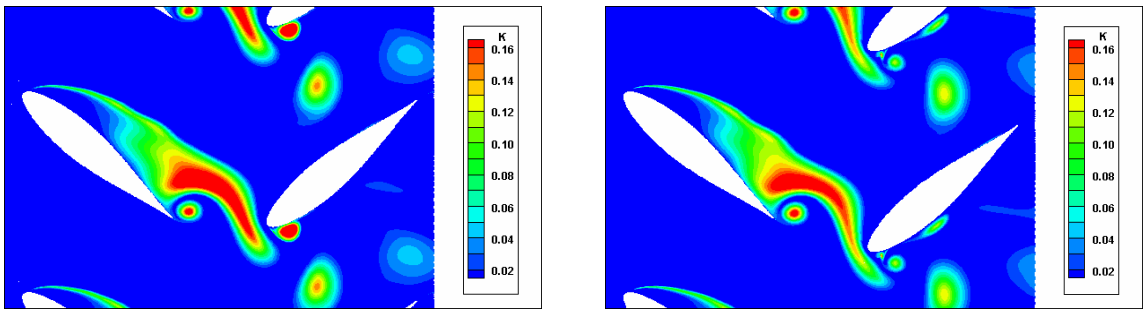

(g) t=0.875T_w (h) t= 1 T_w

Fig. 5.5. Distribution of turbulent kinetic energy in one flow period, without control

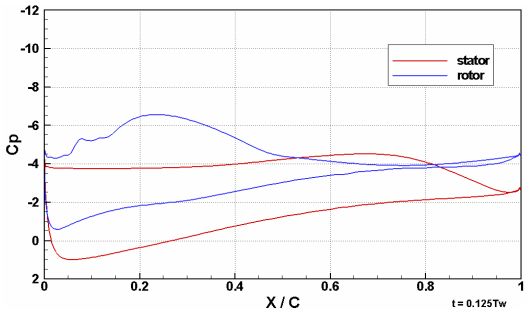

(a) t=0.125T_w

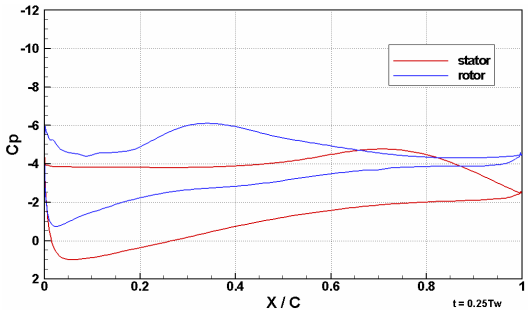

(b) t=0.25T_w

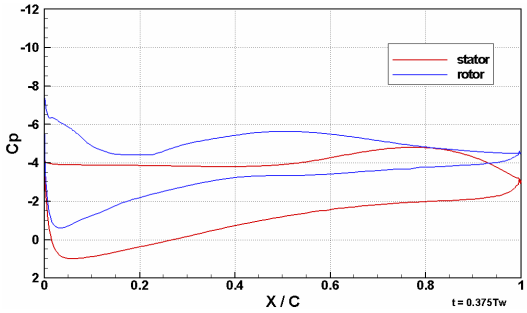

(c) t=0.375T_w

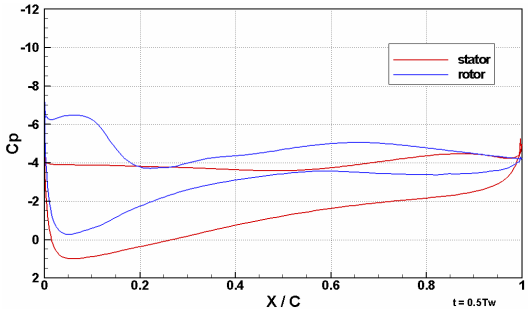

(d) t=0.5T_w

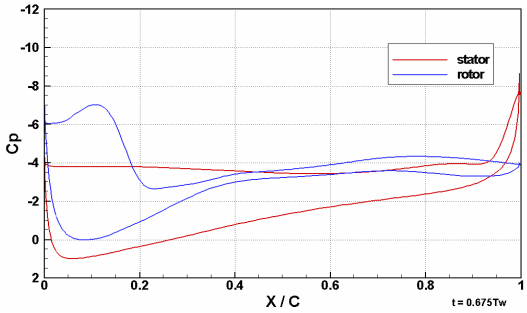

(e) t=0.625T_w

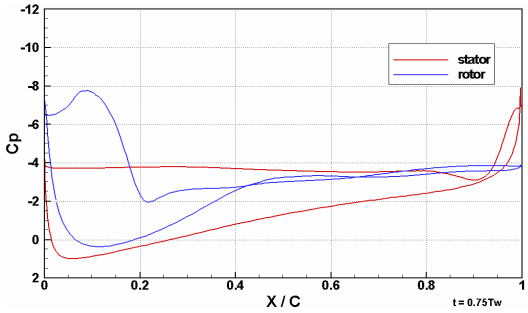

(f) t=0.75T_w

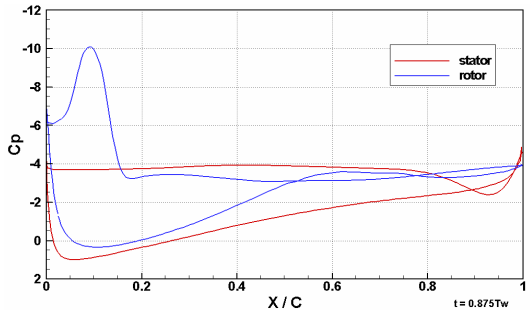

(g) t=0.875T_w

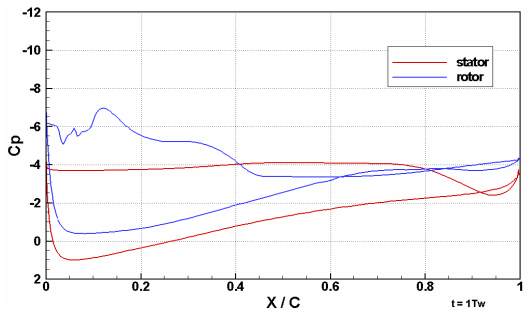

(h) t= 1 T_w

Fig. 5.6. Distribution of pressure coefficients on stator and rotor blades in one flow period, without control

The aerodynamic performances of stator and rotor blades are tabulated below. The lift and drag are non-dimensionalized by $\frac{1}{2}\rho u_\infty^2$.

	Lift Coe. C_l	**Drag Coe. C_d**	**Lift-to-Drag Ratio**
Stator	1.94	1.86	1.04
Rotor	1.49	1.31	1.14

Tab. 5.1. Aerodynamic performances of stator and rotor blades, without control

The loss of the flow is measured by the difference of total pressure coefficient measured at the inlet and the outlet. The coefficient is defined as:

$$\Delta P = \frac{P_{in} - P_{out}}{\frac{1}{2}\rho u_\infty^2}, \tag{5.1}$$

where P_{in} and P_{out} are the total pressure at the inlet and the outlet, respectively.

In this case, the loss of total pressure is 3.224 times the free-stream dynamic pressure $\frac{1}{2}\rho u_\infty^2$. In practice, such an arrangement is obviously inapplicable because it works at extreme part load operation and the flow losses are too high. This deficiency comes from the large separation region on the stator blade, its downstream development and the strong turbulent behavior in the flow field.

The investigation of controlling the massively separated flow in the arrangement using a synthetic jet is carried out and described in the following section.

5.3 Results with Synthetic Jet

In order to investigate the possibility of suppressing the separation and reducing the flow losses in the arrangement, a synthetic jet is set up at 0.1% chord of the stator blade where the flow separates otherwise. The synthetic jet is expelled and ingested from a channel of 1×1.3 mm^2 discretized with 19×21 cells. Near the jet orifice, the computational grid is locally refined. A zoom-in picture of the grid in the vicinity of the orifice is shown in Figure 5.7. The rest

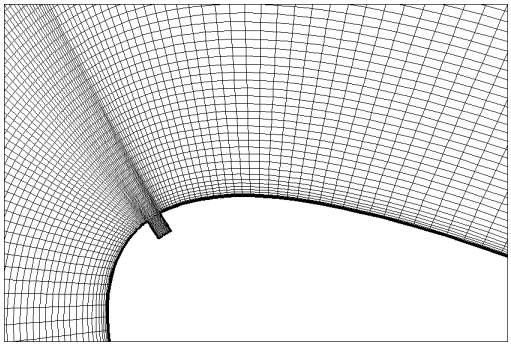

Fig. 5.7. Locally refined computational grid

of the computational domain is discretized in the same way as that shown in Figure 5.2. There are altogether about 154,000 cells in the whole computational domain.

The velocity perpendicular to the jet orifice is prescribed as a step function. Its absolute value is 15m/s. The velocity is uniform along the orifice. According to the conclusion in Chapter 4, the range of efficient frequency concerning the stator-blade control may be near 1.5 to 2 times the frequency $f_c = u_\infty / C\cos\alpha$, i.e. 100 to 132Hz. Therefore, the frequency of excitation at 120Hz is chosen in this work and the results of excitation are given below.

Under the 120Hz frequency of excitation, the leading-edge separation can be effectively suppressed. Figure 5.8 gives the flow pattern for the stator blades at four instants in one flow period T_w, here two periods of excitation T_e. The large separation mode of the flow in the unforced case is transformed into several separation bubbles with reattachment onto the blade surface, except the separation bubble at the trailing edge that sheds up directly into the wake. The dimension of the separation bubbles is at least an order of magnitude lower than the blade dimension and the dimension of the massive separation. The separation bubbles are less energetic than the large separation.

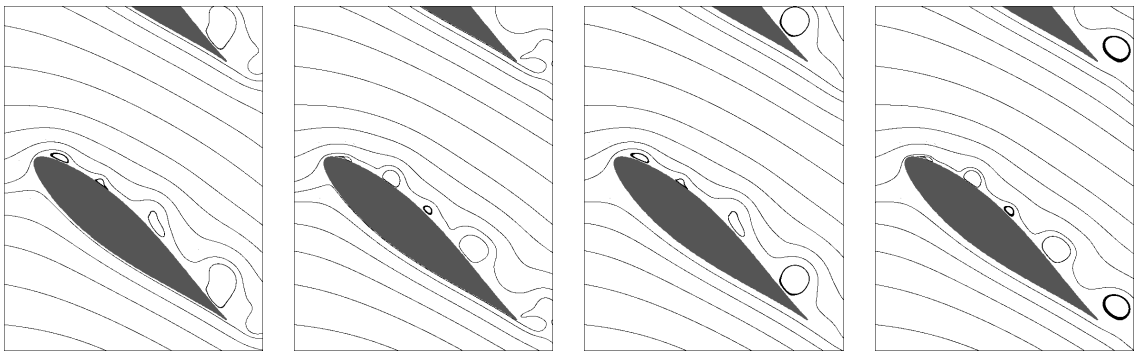

(a) t=0.25T_w (b) t=0.5T_w (c) t=0.75T_w (d) t=1T_w

Fig. 5.8. Stator flow pattern at four instants in one flow period, from excitation of 120Hz and 15m/s

The reorganization of the flow pattern of the stator blades brings favorable changes to the flow field. Firstly, the flow layer in which the separation bubbles are embedded is confined to a thin layer near the wall. The pressure loss can be suppressed to a great extend. Secondly, the separation bubbles are less energetic than the large separation region. The rest of the flow field is less disturbed and remains nearly laminar. They contain high level of turbulent kinetic energy only in their core region. The mixing loss can be, therefore, reduced considerably. Thirdly, the wake of the stator blade is relatively steady as the disturbed stator flow is constrained in a thin layer. The incident flow for the rotor blades is, therefore, more regular.

Figure 5.9 gives the rotor flow pattern at the same instants as in Figure 5.8. In comparison with the pictures in Figure 5.4 for the unforced flow, the incident flow for the

rotor blade changes its direction more gently. The flow on both surfaces of the rotor blade is fully attached. No recirculating region exists in the rotor flow field. The dominating flow loss is the friction loss but not the pressure loss.

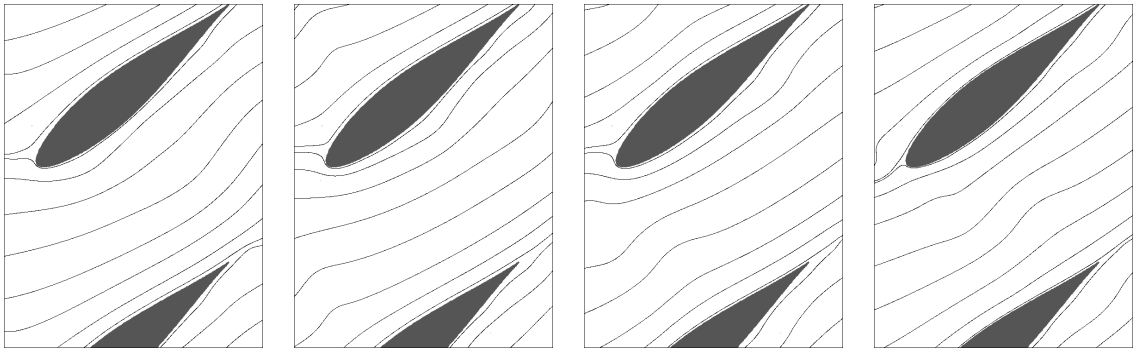

(a) t=0.25T_w (b) t=0.5T_w (c) t=0.75T_w (d) t=1T_w

Fig. 5.9. Rotor flow pattern at four instants in one flow period, from excitation of 120Hz and 15m/s

Figures 5.8 and 5.9 illustrate that the synthetic jet at the frequency of excitation of 120Hz is very efficient in suppressing the massive separation on the stator blade. The massive separation can be transformed into a series of separation bubbles. The flow is well reorganized and its losses are reduced to a large extent. From the figures in Table 5.2 one can observe that the drag coefficients for stator and rotor blades can be reduced by about 50%.

	Lift Coe. C_l	**Drag Coe. C_d**	**Lift-to-Drag Ratio**
Stator	1.60	0.90	1.78
Rotor	1.02	0.66	1.55

Tab. 5.2. Aerodynamic performances of stator and rotor blades, from excitation of 120Hz and 15m/s

The distribution of turbulent kinetic energy resulting from the excitation is shown in Figure 5.10. Figure 5.11 gives the corresponding pressure coefficient distributions on stator and rotor blades. In comparison with the pictures in Figure 5.5, one can find that the turbulence kinetic energy is dramatically suppressed in the whole flow field. The high level of turbulent energy is well confined to be inside the separation bubbles, whereas the remaining flow regions are less energetic and a good laminar state is achieved. The flow losses from the mixing procedure are considerably reduced. The loss of total pressure is 1.186 times the free-stream dynamic pressure, instead of 3.224 in the unforced case.

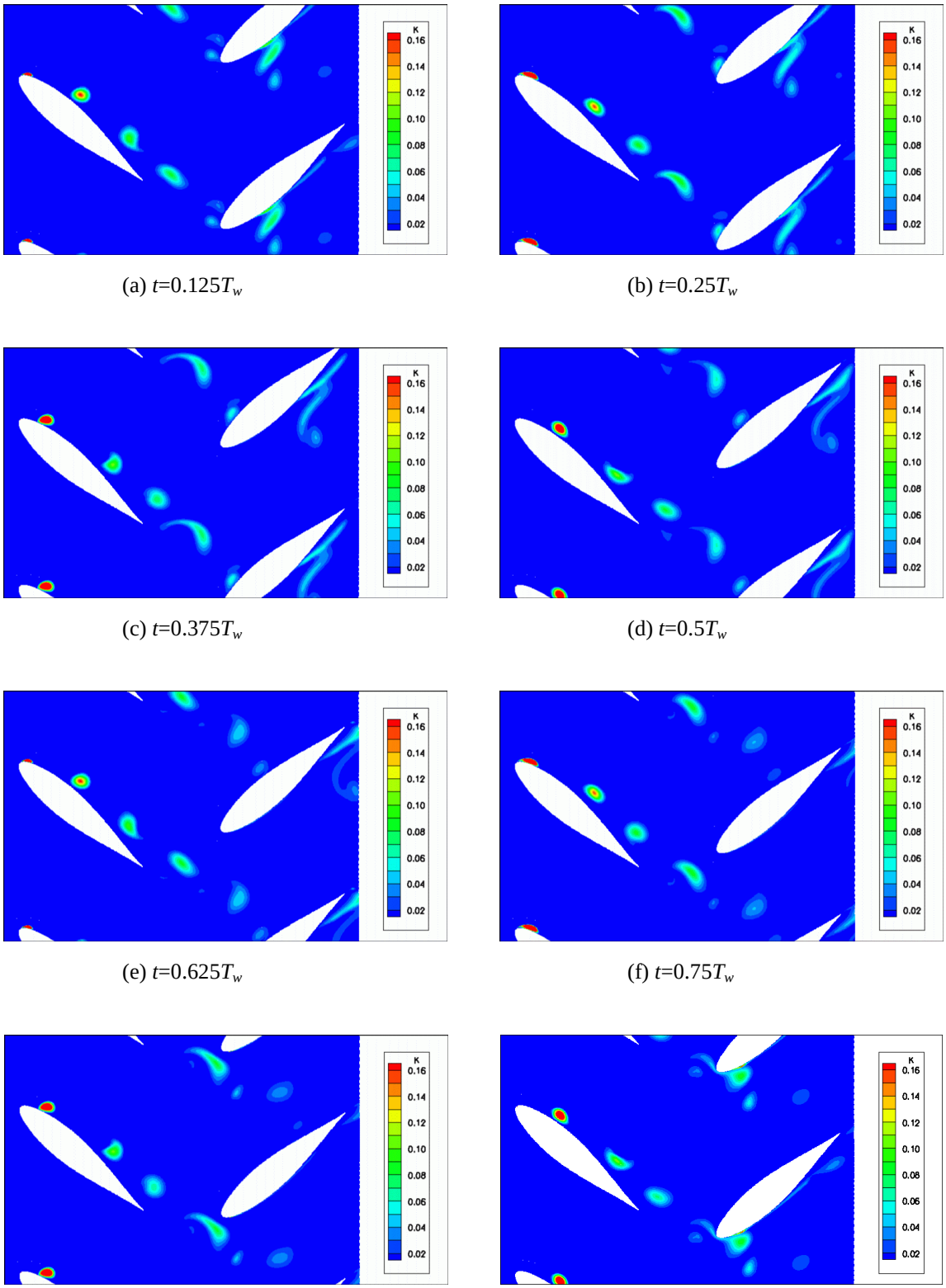

(a) t=0.125T_w (b) t=0.25T_w

(c) t=0.375T_w (d) t=0.5T_w

(e) t=0.625T_w (f) t=0.75T_w

(g) t=0.875T_w (h) t= 1 T_w

Fig. 5.10. Distribution of turbulent kinetic energy in one flow period, from excitation of 120Hz and 15m/s

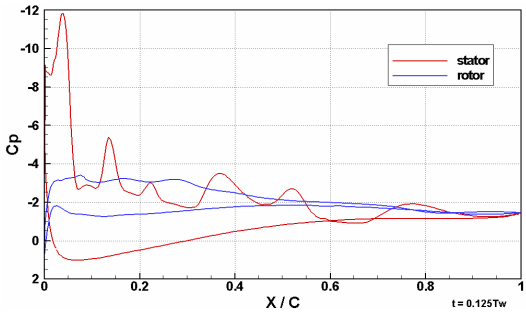

(a) t=0.125T_w

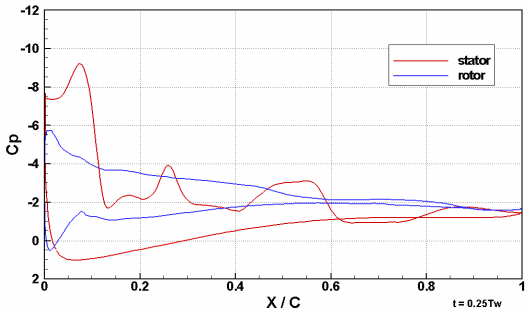

(b) t=0.25T_w

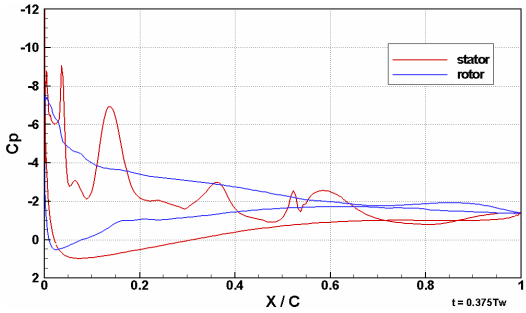

(c) t=0.375T_w

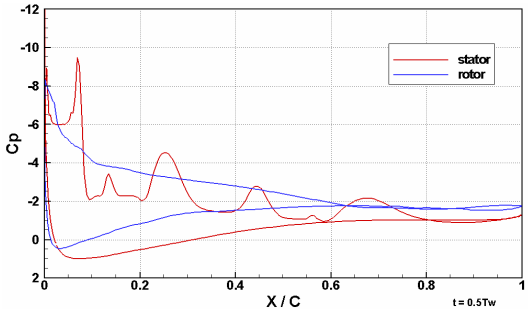

(d) t=0.5T_w

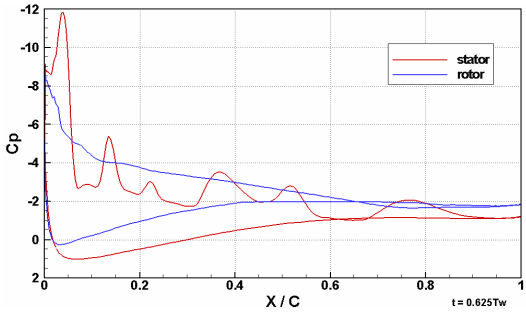

(e) t=0.625T_w

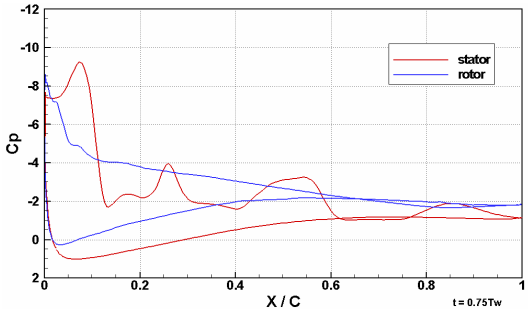

(f) t=0.75T_w

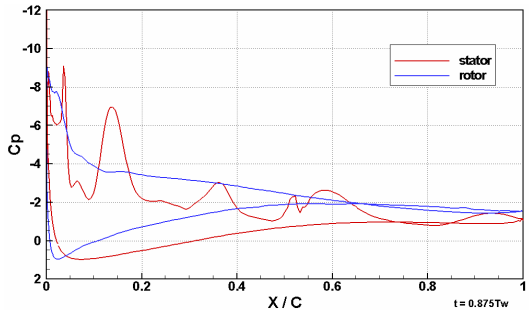

(g) t=0.875T_w

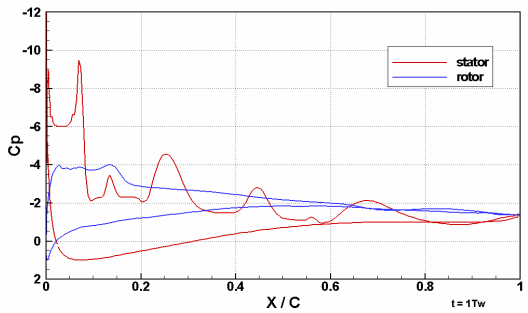

(h) t= 1 T_w

Fig. 5.11. Distribution of pressure coefficients on stator and rotor blades in one flow period, from excitation of 120Hz and 15m/s

5.4 Discussion and Conclusion

The investigation on the stator-rotor arrangement has shown that the synthetic jet performs well in reducing the losses of the cascade flow. The performance of the stator-rotor arrangement can be improved obviously.

The improvement exhibits in several aspects. Firstly, the massive separation at the leading edge of the stator blades is suppressed. Several separation bubbles are formed on the blade through the introduction of the synthetic jet. The separation bubbles are small in size. The flow is reattached in between. These effects prevent the occurrence of large pressure drag. Secondly, the level of turbulent energy in the stator flow field is dramatically reduced. A good laminar state of the flow can be achieved. Therefore, the mixing loss is reduced. Thirdly, the stator wake is well oriented and changes its direction more gently as the flow layer in which the separation bubbles are embedded is confined to a limited range from the blade surface. The stator wake is less disturbed and energetic, which gives a relative good incident condition for the rotor blade. Fourthly, as a result of the well-reorganized stator flow, the rotor flow is fully attached and the turbulent energy is of lower level.

The above-mentioned reasons make it possible that the overall flow losses in such an arrangement are depressed dramatically. Through the synthetic jet, the drag of the single stator or rotor blade can be reduced by about 50% and the loss of total pressure is reduced to be one-third of the value in the unforced case.

Comparing with the stalled airfoil flow, the cascade flow undergoes higher pressure gradient. The dimension of the massive separation on the stator blade is smaller. The overall periodicity of the cascade flow is determined by the frequency of the relative motion and the artificial frequencies. The effect of excitation by the synthetic jet on the cascade flow is obviously better than that on single stalled airfoil.

It can be concluded from the above discussion that the technique of synthetic jet is quite promising in controlling the massive separation in cascade flow. It is more efficient than that of single stalled airfoil. The position of the synthetic jet and the frequency of excitation may be the most important parameters.